Quantitative local structure determination of R,R-tartaric acid on Cu(110): monotartrate and bitartrate phases

D.A.Duncan[1], W. Unterberger[2], D.C. Jackson[1], M.K. Knight[1], E.A. Kröger[2], K.A. Hogan[3], C.L.A. Lamont[3], T.J. Lerotholi[1,4], and D.P. Woodruff[1]

[1]University of Warwick, Coventry, CV4 7AL, UK

[2]Fritz-Haber Institut der MPG, Faradayweg 4-6, D 14195, Berlin, Germany

[3]University of Huddersfield, Queensgate, Huddersfield, HD1 3DH, UK

[4]University of Witwatersrand, PO Wits, Johannesburg, 2050, South Africa

Abstract

The local adsorption site of the monotartrate and bitartrate species of R,R-tartaric acid deposited on Cu(110) have been determined by scanned-energy mode photoelectron diffraction (PhD). In the monotartrate phase the molecule is found to adsorb upright through the O atoms of the single deprotonated carboxylic acid (carboxylate) group, which are located in different off-atop sites with associated Cu-O bondlengths of 1.92±0.08Å and 1.93±0.06Å; the plane of the carboxylate group tilted is by 17±6° off the surface normal. The bitartrate species adopts a 'lying down' orientation, bonding to the surface through all four O atoms of the two carboxylate groups, also in off-atop sites. Three slightly different models give comparably good fits to the PhD data, but only one of these is similar to that predicted by earlier density functional theory calculations. This model is found to have Cu-O bondlengths of 1.93±0.08Å and 1.95±0.08Å, while the planes of the carboxylate groups are tilted by 38±6° from the surface normal.

Keywords: chemisorption; chirality; surface structure; photoelectron diffraction; copper; tartaric acid

1. Introduction

In the last few years there has been increasing interest in the study of chiral molecules adsorbed on surfaces. This work is motivated by the need to produce enantiopure chiral molecules (e.g. [1]) for pharmaceutical applications (e.g. [2]); currently this is generally achieved using homogeneous catalysts that tend to be expensive and difficult to recover. By understanding the way such molecules interact with surfaces one might ultimately identify heterogeneous catalysts for this purpose. Indeed, the addition of chiral molecules, such as tartaric acid, to act as modifiers to heterogeneous catalysts, such as Raney nickel, has proved to be successful in this regard [3, 4, 5]. Tartaric acid (which has two chiral centres, see Fig 1) in its crystalline form was the first material found to have optical activity [6], now known to be associated with the chirality of the molecule. Its adsorption on the Cu(110) surface has been used as a model system for extensive investigation by a range of experimental techniques including low energy electron diffraction (LEED), scanning tunnelling microscopy (STM), Fourier-transform reflection-absorption infrared spectroscopy (FT-RAIRS) [7, 8], and also by density functional theory (DFT) calculations [9, 10, 11]. The FT-RAIRS results, in particular, have identified two different surface species that can be formed through the interaction of tartaric acid with Cu(110) under different conditions, namely monotartrate and bitartrate, depending on whether only one or both carboxylic acid groups are deprotonated to create carboxylate (COO-) groups that can form chemisorption bonds to the surface through the two constituent O atoms. The long-range ordering of these molecules has been of especial interest because of the potential significance of the fact that all the ordered phases are globally chiral, leading to exposed Cu surface regions or 'gaps' in the overlayers that are potential sites for enantiospecific surface chemistry. Several different long-range ordered phases of the monotartrate species have been identified at different coverages and temperatures. At room temperature, a sub-saturation $\begin{pmatrix} 4 & 0 \\ 2 & 3 \end{pmatrix}$ ordered overlayer is formed, which transforms to a $\begin{pmatrix} 4 & 1 \\ 2 & 3 \end{pmatrix}$ phase at higher

coverage. Annealing of this high coverage phase to ~400 K leads to the formation of a $\begin{pmatrix} 4 & 1 \\ 2 & 5 \end{pmatrix}$ monotartrate phase, but similar annealing of the lower-coverage monotartrate phase leads to a $\begin{pmatrix} 9 & 0 \\ 1 & 2 \end{pmatrix}$ bitartrate phase. A recent DFT study [11] concluded that the potential barrier for initial deprotonation, to form the monotartrate species on the Cu(110) surface, is below 0.1eV, whereas the barrier to form the bitartrate species is more than 1 eV, qualitatively consistent with the need for increased temperatures to create the bitartrate. The fact that this conversion only occurs at lower monotartrate coverages is also consistent with the larger 'footprint' of the bitartrate species on the surface, and thus the need for vacant Cu surface sites. STM images of the $\begin{pmatrix} 4 & 1 \\ 2 & 3 \end{pmatrix}$ and $\begin{pmatrix} 9 & 0 \\ 1 & 2 \end{pmatrix}$ phases each show three adsorbate features per unit cell that are proposed to each correspond to a single tartrate species; this implies that the coverages of these phases are 0.25 ML and 0.17 ML respectively [7].

While these previous studies of the Cu(110)/tartaric acid system provide considerable insight into the surface reaction and molecular ordering, none of the experiments provide information on the local adsorption geometry. It has been generally assumed that the deprotonated species bond to the surface in a fashion locally identical to that of the simple carboxylate species formate (HCOO) [12, 13, 14], acetate (CH_3COO) [15], and benzoate (C_6H_5COO) [16] on this surface, with the two O atoms of each carboxylate species occupying near-atop sites relative to two nearest-neighbour Cu surface atoms along the close-packed $[1\bar{1}0]$ rows. This geometry is consistent with the results of the DFT calculations [9]. Of course, in the bitartrate phase, bonding of the molecule through both sets of carboxylate O atoms means that the mismatch of the unstrained surface and molecular geometry imposes constraints on the exact local bonding sites. A similar effect is seen in the simple amino acids, glycine (NH_2CH_2COOH) [17] and alanine (NH_2CHCH_3COOH) [18], which bond through both the deprotonated carboxylate O atoms and the amino N atom, and this three-point bonding on

Cu(110) does force one of the O atoms to adopt a site that is substantially displaced from a local atop geometry. The impact of the four-point bonding of the bitartrate phase is thus an issue of some interest.

Here we present the first direct experimental quantitative determination of the local adsorption site of tartaric acid on Cu(110) for both the monotartrate and bitartrate conformers using scanned-energy mode photoelectron diffraction (PhD), the same technique that has been used in the past to determine the local adsorption geometry of other carboxylic acid species on copper surfaces [13, 14, 15, 16, 17, 18]. The PhD technique [19, 20] exploits the coherent interference of the directly-emitted component of the photoelectron wavefield, from a core level of an adsorbate atom, with components of the same wavefield that are elastically backscattered by the nearby (mainly substrate) atoms. By measuring the photoemission in specific directions as a function of photon energy, and hence photoelectron energy and wavelength, the scattered wavefield components shift in and out of phase relative to the directly emitted component; the resulting modulations in the detected photoemission intensity, which depend on the scattering pathlengths, thus provide information on the relative emitter-scatterer atomic positions. These modulations can be simulated for different structural models using multiple scattering calculations, and by modifying the structure until one achieves good agreement with the experimental measurements, the local adsorption geometry around the emitter can be determined.

2. Experimental details

The experiments were conducted in an ultra-high vacuum surface science end-station equipped with typical facilities for sample cleaning, heating and cooling. This instrument was installed on the UE56/2-PGM-2 beam line of BESSY-II, which comprised a 56 mm period undulator followed by a plane grating monochromator [21]. The sample could be rotated about its surface normal (to change the azimuthal angle) and about its vertical axis (to change the polar angle), allowing (simultaneous) variation of incidence and electron collection directions.

Sample characterisation *in situ* was achieved by LEED, and by SXPS (soft X-ray photoelectron spectroscopy) using the incident synchrotron radiation. The SXPS and PhD data were measured using an Omicron EA-125HR 125 mm mean-radius hemispherical electrostatic energy analyser, equipped with seven-channeltron parallel detection, which was mounted at a fixed angle of 60° to the incident radiation, in the same horizontal plane as that of the polarisation vector of the incident radiation.

A clean, well-ordered Cu(110) surface was prepared from an oriented and polished crystal slice by the usual combination of Ar^+ ion bombardment and brief annealing to 950 K, to give a sharp (1x1) LEED pattern and a SXP spectrum devoid of impurities. R,R-tartaric acid dosing of the sample was achieved by heating the powder (99% purity, Sigma Aldrich) to 400 K. Dosing with the sample held at 400 K yielded a clear $\begin{pmatrix} 9 & 0 \\ 1 & 2 \end{pmatrix}$ LEED pattern, consistent with that expected for the bitartrate phase. Dosing with the sample at room temperature, the conditions known to produce monotartrate layers, yielded a different LEED pattern of poor quality; it was not possible to determine whether the pattern corresponded to the $\begin{pmatrix} 4 & 0 \\ 2 & 3 \end{pmatrix}$, $\begin{pmatrix} 4 & 1 \\ 2 & 3 \end{pmatrix}$, or $\begin{pmatrix} 4 & 1 \\ 2 & 5 \end{pmatrix}$ phase.

PhD modulation spectra were obtained by measuring photoelectron energy distribution curves (EDCs) of the O 1s peaks at 4 eV steps in photon energy, over the photoelectron kinetic energy range of 50-350 eV for a number of different polar emission angles in the [001] and $[1\bar{1}0]$ azimuths. These data were processed following our general PhD methodology (e.g. [19,20]) in which the individual EDCs are fitted by a sum of Gaussian peaks, a Gauss error function, and a template background. The integrated areas of each of the individual chemically-shifted component peaks were then plotted as a function of photoelectron kinetic energy, and these plots were used to define a smooth spline which represents the non-diffractive intensity and instrumental factors. The spline was then subtracted from, and used to normalise, the integrated areas, to provide the final PhD

modulation spectrum.

3. Results

3.1. SXPS Characterisation

The O1s and C1s SXP spectra from the prepared monotartrate and bitartrate phases are shown in Fig 2. These SXP spectra clearly show that the coverage in the monotartrate phase measured here is significantly larger than that of the bitartrate phase. Comparison of the photoemission intensity ratio of the O 1s and Cu 3s peaks obtained from a saturated Cu(110)(2x1)-O surface (O coverage 0.5 ML), with those from the tartrate-covered surfaces provides coverage estimates of 0.3 and 0.2 ML for the monotartrate and bitartrate phases respectively. The spectra of Fig. 2 show (at least) two clearly-resolved chemically-shifted components in both the O 1s and C 1s photoemission, with a very significant difference in the relative intensities of the two O 1s components between the monotartrate and bitartrate species. The fact that there is such a change is consistent with the different number of deprotonated carboxylic groups in these two species, as identified in the previous FT-RAIRS study.

The assignment of the two peaks in the C 1s SXP spectra is relatively straightforward by comparison with spectra from other molecules containing both a carboxylic acid or carboxylate species, and one or more four-fold coordinated C atoms. The higher kinetic energy peak may be attributed to the middle carbon atoms, C(2) and C(3) (Fig. 1), which are bonded to the alcohol groups, while the lower kinetic energy peak is associated with the outer carbon atoms, C(1) and C(4) that are part of the carboxylic acid/carboxylate groups. One surprising feature of the C 1s spectra is that the peak at lower kinetic energy appears to be consistently weaker than the peak at higher kinetic energy, although according to this assignment, both peaks arise from 2 C atoms in the tartrate species. This effect has also been observed in C 1s spectra in many other adsorbed (deprotonated) species produced by reaction with carboxylic acids, notably acetic acid on Cu(110) [15], glycine on Cu(111) [22] and Pd(111) [23], serine on

Cu(110) [24], and alanine on Cu(110) [25, 26], and must be attributed to loss of intensity in one of the peaks to shake-up satellites; the shoulder visible in the spectra at lower kinetic energy is consistent with this interpretation.

The assignment of the O 1s SXP spectral peaks in the bitartrate species is also clear. In this species there are four O atoms in carboxylate groups (O(1), O(2), O(5) and O(6)), and two O atoms on the OH groups (O(3) and O(4)); this would lead us to expect two peaks with an intensity ratio of 2:1, consistent with the spectrum in Fig. 2. We can therefore assign the higher kinetic energy peak to carboxylate O atoms and the lower kinetic energy peak to OH species. However, in the case of the monotartrate O1s XP spectrum (Fig 2a) there are two peaks with approximately the same area, but the molecule contains six O atoms in four different bonding states. As the monotartrate retains two O atoms in OH species (O(3) and O(4)), and two O atoms in the carboxylate group (O(1) and O(2)), these four O atoms may be expected to lead to peaks at the same energies as the two peaks in the bitartrate spectrum. The implication is therefore that the two O atoms in the remaining carboxylic acid group, namely the C=O and C-OH species, must have O 1s chemical shifts similar to the carboxylate and OH species of the bitatrate. It seems most reasonable to assign them to these two components in this order although, as we shall see, for the purposes of our PhD structure investigation, the ordering of these assignments proves to be unimportant.

3.2. PhD results: qualitative evaluation

The objective of the PhD analysis is to determine the local adsorption structure of the two different tartrate species on the Cu(110) surface. The strongest elastic scattering contributions to PhD modulations arise from scattering by near-neighbour Cu substrate atoms (which are much stronger scatterers than the O, C and H atoms within the molecule). PhD data from the adsorbate atoms that are bonded to the surface are thus the primary source of structural information, and in the present case these are expected to be the O atoms of the deprotonated carboxylate groups. For this reason we focus our

analysis on the PhD modulation spectra from the higher kinetic energy component of the O 1s emission spectra.

Proper analysis of PhD in order to extract quantitative structural information relies on the use of multiple scattering simulations, but visual inspection of the raw experimental data can often provide some qualitative information. The experimental PhD spectra associated with the higher kinetic energy O 1s peak recorded from both the monotartrate and bitartrate species are shown in Fig 3. The PhD spectra from the O 1s peak at lower kinetic energy were devoid of any obvious modulations, consistent with our expectation that this emission is from O atoms that are relatively far from the surface and lack any near-neighbour Cu scatterer atoms. A striking feature of the data of Fig. 3 is the remarkable similarity of the spectra from the two different species. One might infer from this that the two structures are identical, yet our SXP spectra and the associated coverage estimates, as well as the previously published FT-RAIRS results using similar preparation methods [7], clearly indicate that the two surface species are different, while the FT-RAIRS data and STM images further indicate that the two molecular orientations differ. It is therefore difficult to see how the two adsorption geometries can be equivalent. The different LEED patterns observed in the present work also reinforce the view that we are studying different surface phases, but LEED tends to be dominated by the diffraction pattern of those regions of the surface that show the best long-range order, which may be a minority phase on the surface. SXPS, on the other hand, averages over the whole surface, so the clear difference in these spectra recorded from the two different methods of surface preparation are indicative of the surfaces being predominantly covered by different species.

In fact a strong similarity in PhD data from the two species is to be expected. We have already noted that all the bonding carboxylate O atoms (two in the monotartrate, four in the bitartrate) are likely to adopt near-atop sites. The different constraints of the anticipated two-point and four-point bonding geometries, involving some mismatch between interatomic distances on the

surface and within the undeformed molecule, would lead us to expect some subtle differences in the O bonding sites, but after averaging over the sites of the inequivalent atoms in the molecules, these differences may have only a modest effect on the resulting PhD data.

On further qualitative observation is that the dominant long range periodicity of the modulations seen in data recorded at and near normal emission is quite similar to that seen from simple deprotonated carboxylates on Cu(110) [14, 15,16]. This strongly suggests that the emitter O atoms are in similar near-atop sites and at similar Cu-O bondlengths of ~ 1.90-1.95 Å. However, the fact that the modulation amplitudes do not decrease substantially with increasing emission angle may suggest that the emitter O atoms are significantly more displaced from exact atop sites than is found to be the case for the simple carboxylates on Cu(110).

3.3. PhD results: quantitative structure determination

In order to achieve a proper quantitative analysis of the PhD data, multiple scattering simulations for different structural models were performed using the computer codes developed by Fritzsche [27, 28, 29]. These are based on the expansion of the final state wave-function into a sum over all scattering pathways that the electron can take from the emitter atom to the detector outside the sample. The level of agreement between the theoretical and experimental modulation amplitudes is quantified using an objective reliability factor (*R*-factor) [19, 20] defined in a fashion closely similar to that proposed by Pendry for quantitative LEED studies [30]. The *R*-factor is defined such that a value of 0 corresponds to perfect agreement, and a value of 1 to uncorrelated data. The lowest value achievable in practice depends on the complexity of the structure and the amplitude of the modulations, but typically falls in the range 0.2-0.4.

In the present case the structural optimisation to locate the best-fit structure is complicated by the large number of structural parameters with at least two

inequivalent O emitter sites in each molecule (creating a multidimensional hyperspace). In order to search for the global minimum of the *R*-factor in this parameter space, and to try to avoid convergence on local minima, structural models were first explored using a particle swarm optimisation algorithm [31]. Having located potential global minima by this approach, an adapted Newton-Gauss algorithm was used to further optimise the structures. Precision estimates associated with the individual structural parameters were obtained using our standard methodology of defining a variance of the minimum value of the *R*-factor associated with a best-fit structure, R_{min} [32]. All parameters values giving structures with *R*-factors less than R_{min} + Var(R_{min}) are regarded as falling within one standard deviation of the best fit structure. In the structure determination for both the monotartrate and the bitartrate the molecule was assumed to adsorb intact with similar intramolecular bondlengths and bond angles to those in the tartaric acid crystal structure [33]. The atomic coordinate systems was defined with the *x*, *y* and *z* axes along, respectively, $[1\bar{1}0]$, [001] and the outward surface normal, [110].

3.3.1 Monotartrate on Cu(110)

In the PhD simulations for the monotartrate species on Cu(110), emission from three O atoms was assumed to contribute to the higher photoelectron kinetic energy and thus to contribute to the measured PhD modulations; these are the two O atoms of the carboxylate group, and one of the two O atoms of the carboxylic acid group (-COOH). The exact location of this third O atoms proves to have very little influence on the PhD spectra, being located significantly further from the surface than the bonding carboxylate O atoms, so it is unimportant whether this emitter atom is at the C=O or C-O-H location in the molecule. Because the molecule is chiral, the two O atoms in the carboxylate group are not symmetrically identical, with only one of these being adjacent to the neighbouring alcohol group; all three emitter O atoms were therefore allowed to occupy inequivalent sites.

In order to explore the multidimensional parameter hyperspace the molecule was allowed to be displaced independently in the *x*, *y* and *z* directions, and the orientation of the plane of the carboxylate group was allowed to tilt with respect to, and rotate about, the surface normal. The PhD technique is generally rather insensitive to the position of intramolecular (low mass number) scatterers, so the sensitivity to variations in the *x*, *y* and *z* position of the whole molecule, and to the rotation ($\varphi_{(COO)}$ relative to the $[1\bar{1}0]$ direction) and tilt ($\theta_{(COO)}$ relative to the surface normal) of the plane of the carboxylate group, arises primarily from their effect in changing the vector between the O atoms of the carboxylate group and their nearest Cu atoms; there is also a much weaker dependence on the location of these O atoms relative to the nearest-neighbour carboxylate C atom. The position of the third (carboxylic acid) emitting O atom is effectively varied by the rotation of the three C-C bonds, but the calculations were found to have no sensitivity to the position of this emitter atom as long as it was a significant distance from the substrate. In addition, the nearest-neighbour Cu atoms to the carboxylate O atoms were allowed to relax in z independently relative to the underlying crystal, as was the whole first layer of Cu atoms.

The best fit structure that was found is shown schematically in Fig. 4, together with a comparison of the simulated and experimental PhD spectra. The corresponding *R*-factor value for the full set of spectra measured in 11 different directions is 0.32. Note that several of the experimental spectra show quite weak modulations and thus a poor signal-to-noise ratio. If these spectra are omitted from the theory-experiment comparison, and the *R*-factor is calculated only for the 5 spectra showing the strongest modulations, the *R*-factor drops to a value of 0.23. The Cu-O bondlengths in this structural solution are 1.92±0.08Å and 1.93±0.06Å for the two carboxylate O atoms (the error estimates being based on the full set of 11 spectra). The values of all the structural parameters in this model are shown in table 1.

3.3.1 Bitartrate on Cu(110)

For the multiple scattering PhD simulations from the bitartrate species, we assume that the four carboxylate O atoms are the emitters that contribute to the PhD spectra. In this case too, the chirality of the molecule means that the two O atoms in a single carboxylate group need not occupy locally equivalent sites; indeed, the mismatch of interatomic spacings in the molecular footprint and in the underlying Cu(110) structure means that some inequivalence is to be expected. However, as the molecule does have 2-fold rotational symmetry, the diagonally-related O atoms (O(1)/O(6) and O(2)/O(5) of Fig. 1) may be expected to occupy equivalent adsorption sites. Strictly, this is only true if the 2-fold rotation axis of the molecule coincides with one of the 2-fold rotation axes of the underlying surface, but we do make this assumption. The molecule is assumed to bridge two adjacent close-packed $[1\bar{1}0]$ Cu rows on the surface.

These two constraints have two implications in the geometry of the molecule. Firstly, the C(2)-C(3) bond in the middle of the molecule must be parallel to the surface. Secondly, the molecule must be centred over a hollow site (directly atop a second-layer Cu atom) or over a long-bridge site (midway between two adjacent Cu atoms along [001], because these are the two positions having 2-fold rotational symmetry that lie between the close-packed $[1\bar{1}0]$ Cu rows. Note that the assumption that the intramolecular bond angles remain the same as in the intact molecule also implies that the COO plane must be tilted relative to the surface normal by more than 19°.

A global structural search was pursued including all C and O atoms; all our PhD calculations neglect the extremely weak scattering from H atoms. The two symmetry-constrained models with the molecule centred over hollow and long-bridge sites (as seen in Fig 6 and Fig 7 respectively), were explored independently. The centre of the molecule was allowed to vary in *z*, while the carboxylate groups were allowed to rotate around the adjacent C-C (C(1)-C(2) and C(4)-C(3)) axes ($\varphi_{(COO)}$), and to tilt with respect to the surface normal

($\theta_{(COO)}$); the whole molecule was also allowed to rotate relative to the surface normal about its centre ($\varphi_{tartaric}$). The Cu atoms closest to the emitting O atoms were also allowed to relax by small amounts in the *y* and *z* directions, while the emitting O atoms were allowed to vary independently in *x* by a small amount. Three competing models with comparably-favourable *R*-factors were found through this search. Two of the models are centred over the hollow site while the third has the molecule centred on the long-bridge site.

Of the two hollow-site models, one is found to have a tilt angle of the COO plane of only 38±6° relative to the surface normal and we refer to this as the 'upright' hollow model. The associated Cu-O bondlengths are 1.94±0.06Å and 1.95±0.09Å, and the *R*-factor value is 0.45, the highest of the three preferred models. This structure is shown schematically in Fig. 5, together with a comparison of the experimental and simulated PhD spectra. The other two models, one with the molecule in the hollow site ('flat' hollow), the other in the bridge site, are shown in Figs 6 and 7, together with the associated comparisons of the theoretical and experimental PhD spectra. Despite the differences in the lateral position of the molecule as a whole, the local positions of the bonding O atoms with respect to the substrate Cu atoms are essentially identical, thus leading to closely similar PhD spectra. The Cu-O bondlengths in the two models are 1.93±0.08Å/1.95±0.08Å and 1.94±0.07Å/1.97±0.09Å; both models give an *R*-factor of 0.43. These two models have the COO planes comparatively flat on the surface, with a tilt of 70±10° relative to the surface normal.

The comparatively high *R*-factors found in these bitartrate structures can be attributed to the relatively poor signal-to-noise ration of the PhD spectra that arise, at least in part, from the lower molecular coverage (by a factor of ~2), and the thus weaker photoemission signal, than that of the monotartrate phase.

4. General discussion and conclusions

Here we have presented the results of the first direct structural information for the

local adsorption site of tartaric acid on Cu(110). As expected, the bonding carboxylate O atoms in the monotartrate and bitartrate phase are found to occupy similar near-atop sites, with no significant differences in Cu-O bondlengths (1.92±0.08/1.93±0.06Å and 1.93-1.97±0.06-0.09Å, respectively). These values are comparable to those found in DFT calculations for the bitartrate species (1.96-1.98 [9] and 1.92-2.01 Å [11]), and to experimentally-determined values for other species on Cu(110) that form a chemisorption bond through their carboxylate O atoms; 1.90±0.03Å for formate on Cu(110) [14], 1.91±0.04Å for acetate [15], 1.91±0.02Å for benzoate [16], and 2.02±0.04Å/2.00±0.04Å for glycinate [17], and 1.90-2.04±0.03Å for alaninate [18]. Interestingly, the bondlengths found for the monotartrate, which bonds to the surface only through one carboxylate species, is essentially identical to those of the simple carboxylates that bond in the same way, while the slightly longer bondlength seen for bitartrate with a four-point bonding to the surface is also seen in the two amino acids with three-point bonding. Whether this marginally-significant difference is due to the geometrical constraints or through-metal effects on the near-neighbour bonding Cu atoms is unclear.

Based on the PhD data analysis alone we are unable to distinguish between the three competing bitartrate models. We note, however, that the published DFT calculations [9, 11] show the bitartrate centred on the hollow site which would exclude our bridge site solution (Fig.7), although it is not clear that the bridging model was explicitly tested in these calculations. Although none of the DFT investigations report specific values for the orientation of the COO plane in the bitartrate calculations, the schematic diagrams presented in these papers indicate the tilt angles from the surface normal are small. The ‘upright’ hollow geometry of Fig. 5 is thus the one model that is consistent with both the PhD data and the results of the DFT calculations; as such it is the most probable structure.

Acknowledgements

The authors acknowledge the benefit of useful discussions with Rasmita Raval and Karsten Horn, and preliminary assistance from Philipp Schmidt, regarding the

preparation of the surfaces investigated here. Partial support of the Engineering and Physical Sciences Research Council (UK) for this work is acknowledged. The computing facilities were provided by the Centre for Scientific Computing of the University of Warwick with support from the Science Research Investment Fund.

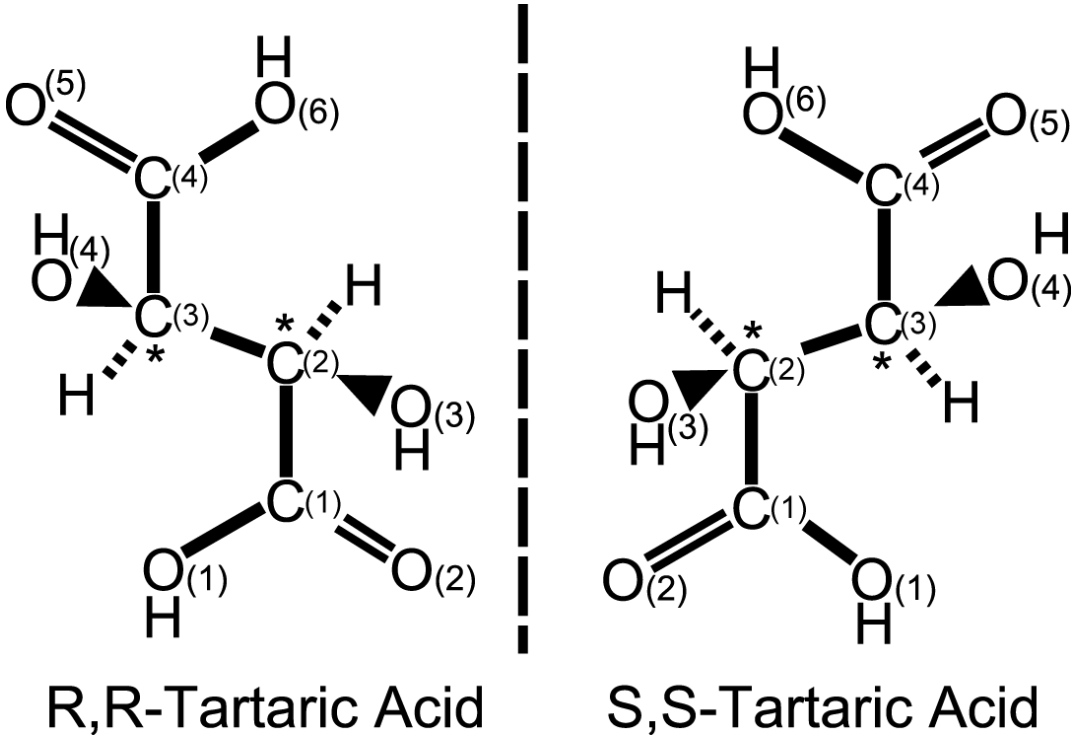

Figure 1: Schematic representation of the two chiral forms of tartaric acid with the chiral centres denoted by '*'. The molecule on the left is the R,R-enantiomer that was used in this study and on the right is the mirror image, the S,S-enantiomer.

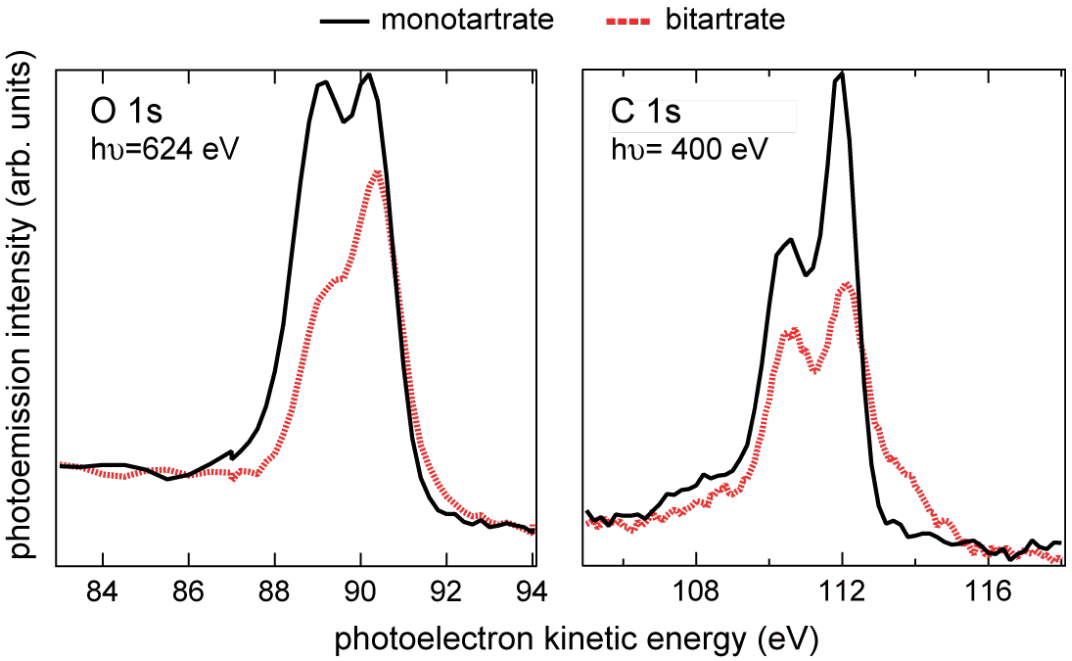

Figure 2: O 1s and C 1s SXP spectra of the monotartrate and bitartrate phases on Cu(110). The C 1s spectra for the bitartrate phase shows a small shoulder at high kinetic energy, attributed to atomic carbon resulting from partial decomposition of tartaric acid. All spectra were measured at normal emission.

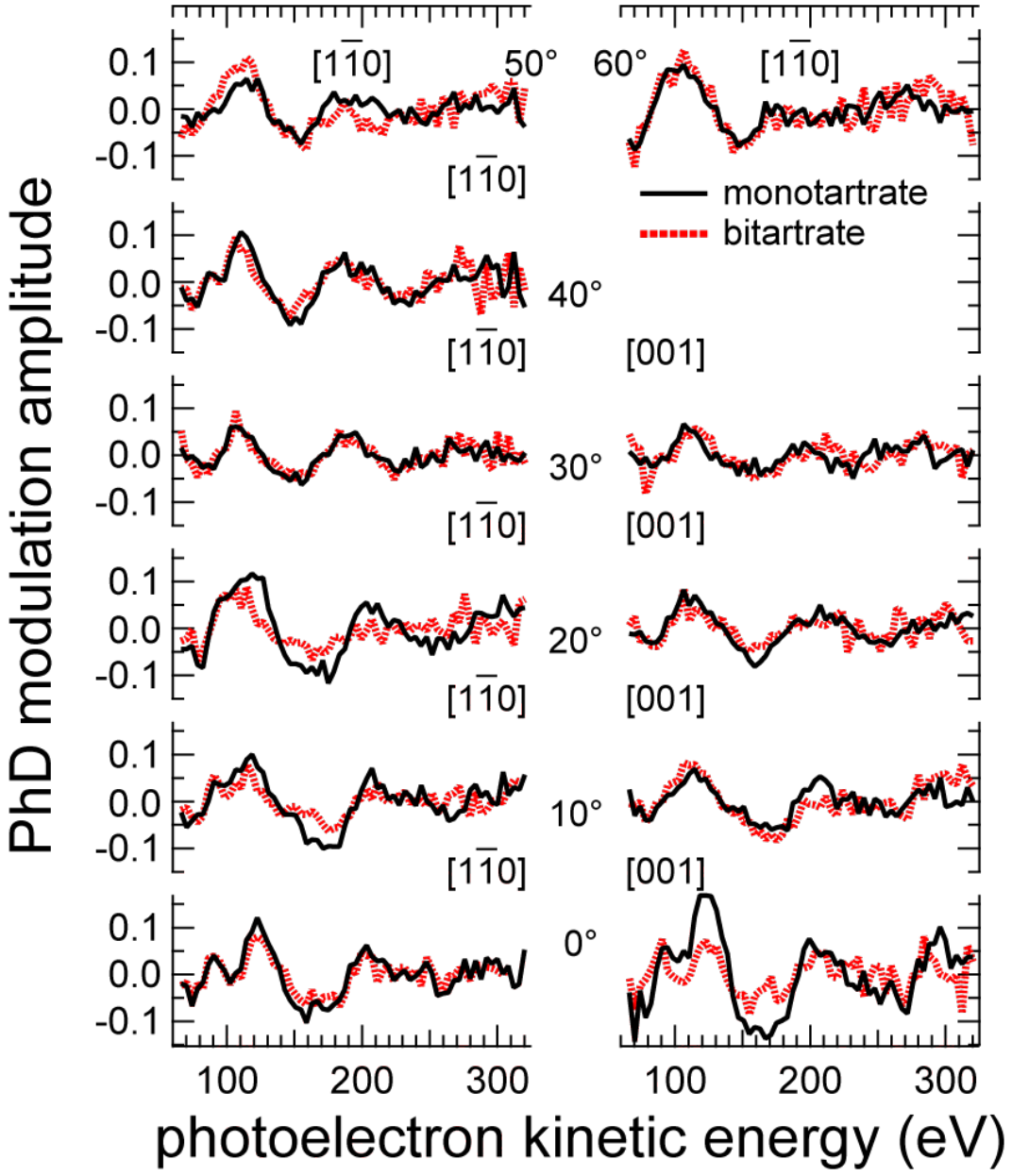

Figure 3: Comparison of the experimental PhD spectra from the mono- and bi-tartrate phases on Cu(110) for several polar and azimuthal emission directions. Only the 11 spectra with the strongest modulations are shown.

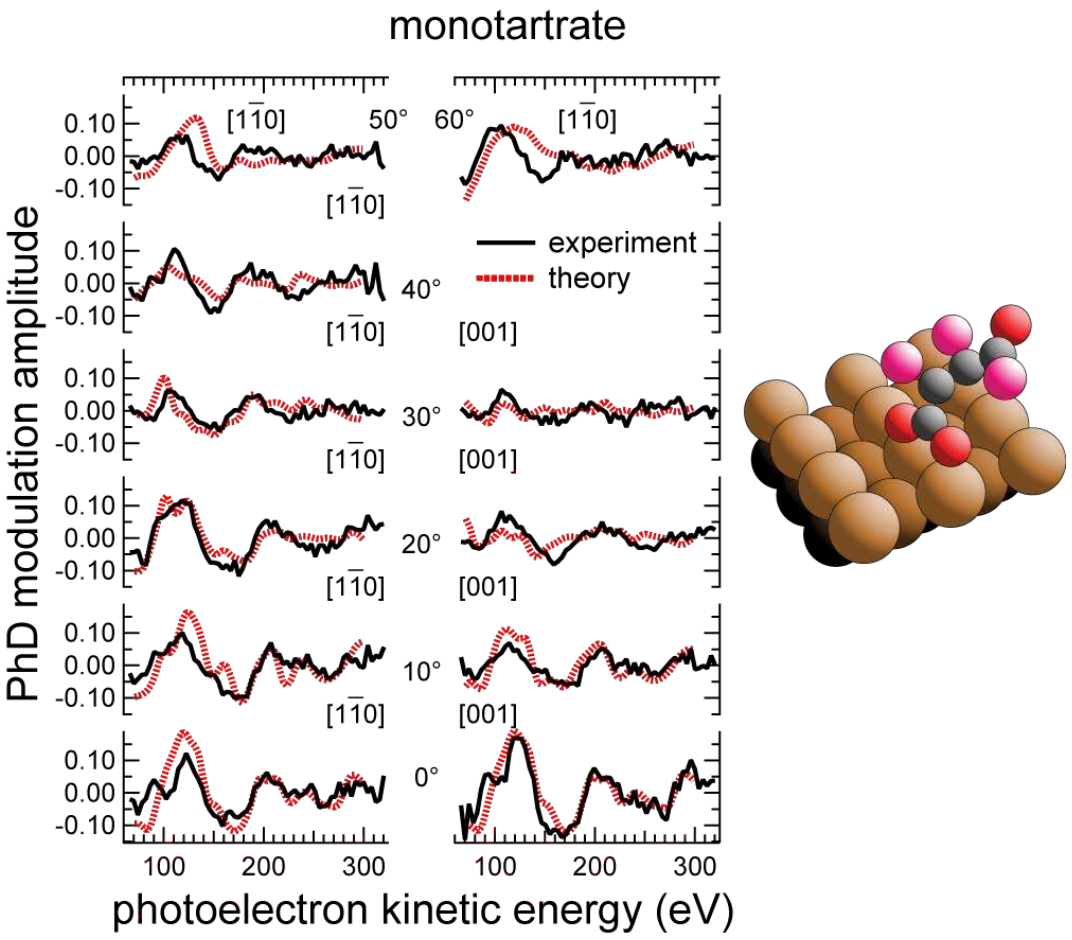

Figure 4: Comparison of the experimental PhD spectra from the higher kinetic energy O 1s peak (Fig. 2) and the results of the simulations for the best-fit structural model for the monotartrate species on Cu(110). On the right is shown a schematic representation of the adsorption geometry. The C atoms are shown in black, while the O emitter atoms contributing to the higher kinetic energy O 1s peak are shaded red. The other O atoms are shaded pink. The (weakly-scattering) hydrogen atoms are not shown, as they were not included in the multiple scattering calculations.

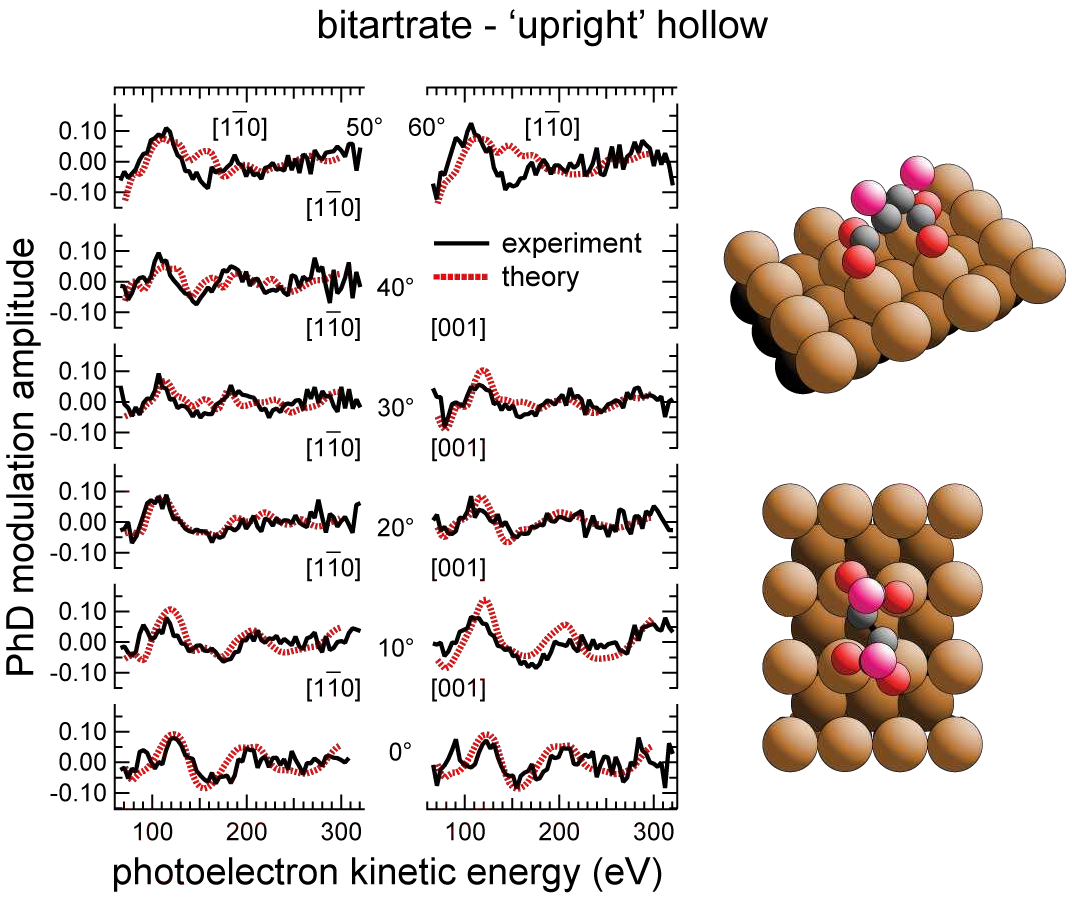

Figure 5: Comparison of the experimental PhD spectra from the higher kinetic energy O 1s peak (Fig. 2) and the results of the simulations for the best-fit bitartrate ‘upright’ hollow structure on Cu(110). A schematic representation of the adsorption geometry is shown on the right in perspective and plan views. The C atoms are shown in black, while the O emitter atoms contributing to the higher kinetic energy O 1s peak are shaded red. The other O atoms are shaded pink. The (weakly-scattering) hydrogen atoms are not shown, as they were not included in the multiple scattering calculations.

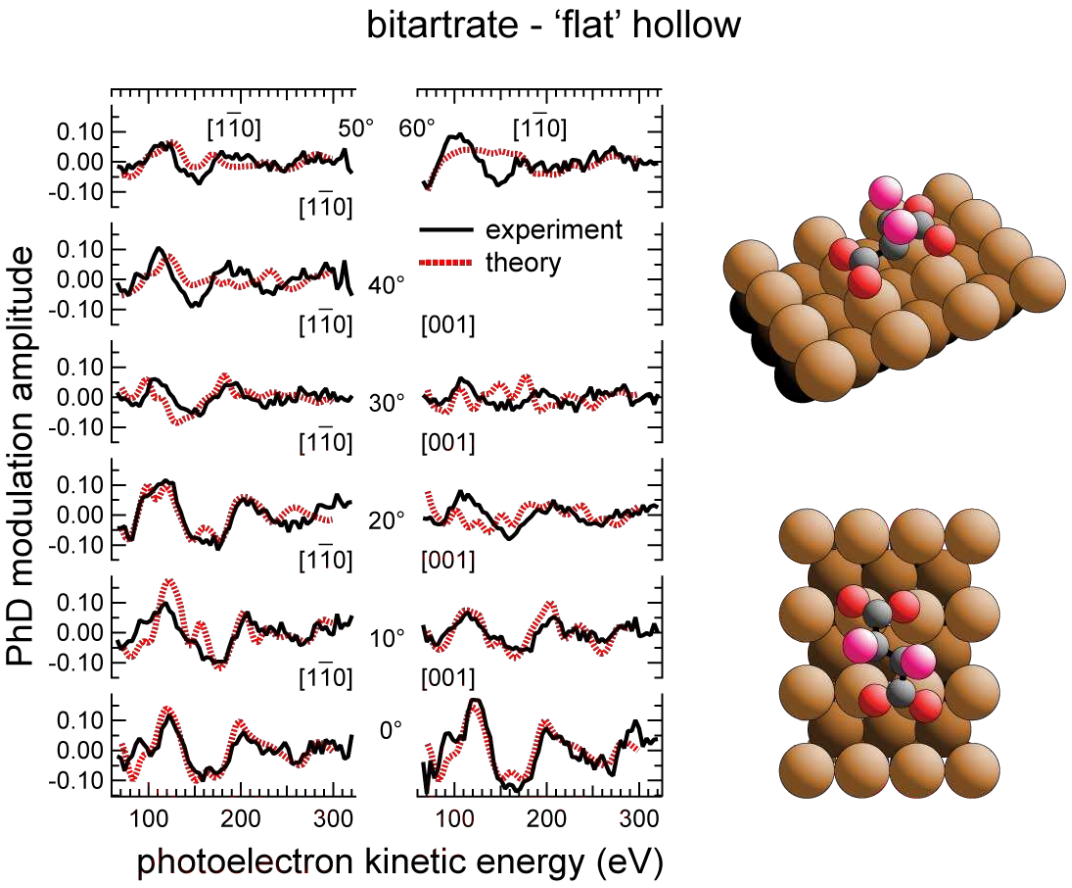

Figure 6: Comparison of the experimental PhD spectra from the higher kinetic energy O 1s peak (Fig. 2) and the results of the simulations for the best-fit bitartrate 'flat' hollow structure on Cu(110). A schematic representation of the adsorption geometry is shown on the right in perspective and plan views. The C atoms are shown in black, while the O emitter atoms contributing to the higher kinetic energy O 1s peak are shaded red. The other O atoms are shaded pink. The (weakly-scattering) hydrogen atoms are not shown, as they were not included in the multiple scattering calculations.

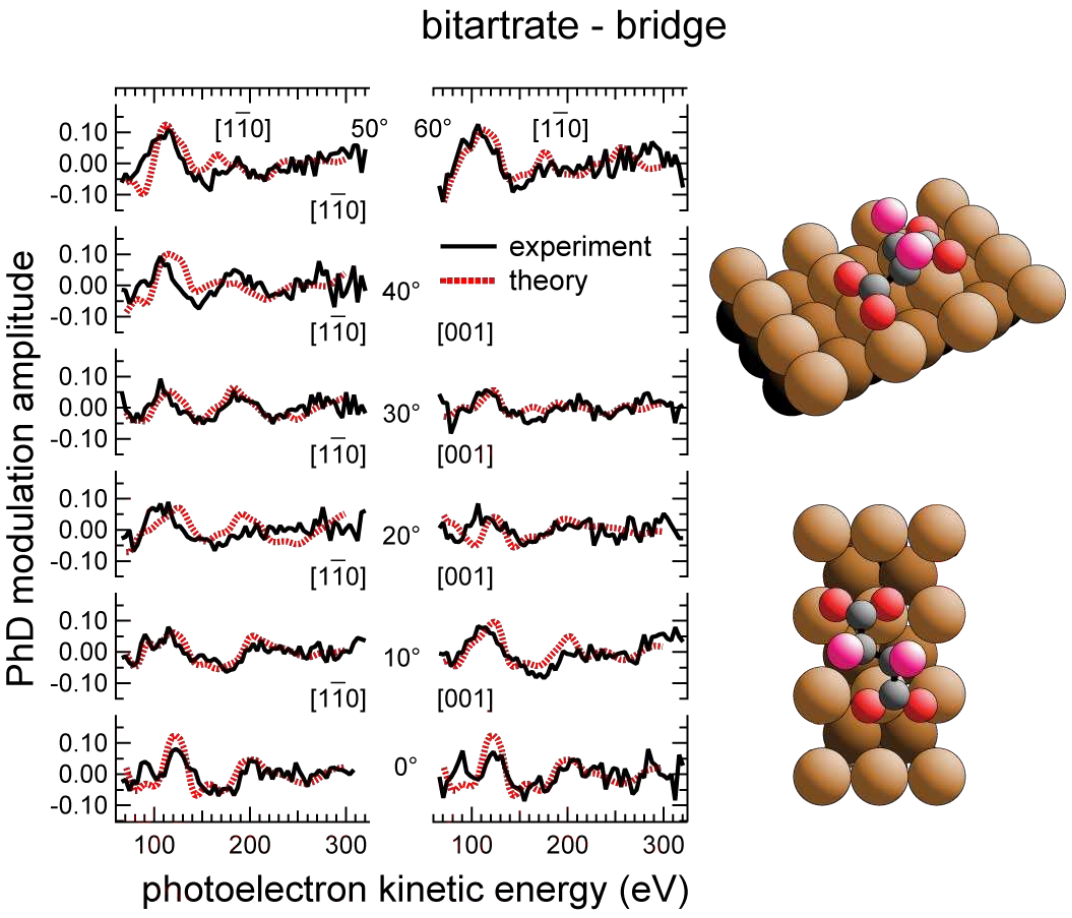

Figure 7: Comparison of the experimental PhD spectra from the higher kinetic energy O 1s peak (Fig. 2) and the results of the simulations for the best-fit bitartrate bridge structure on Cu(110). A schematic representation of the adsorption geometry is shown on the right in perspective and plan views. The C atoms are shown in black, while the O emitter atoms contributing to the higher kinetic energy O 1s peak are shaded red. The other O atoms are shaded pink. The (weakly-scattering) hydrogen atoms are not shown, as they were not included in the multiple scattering calculations.

Table 1: Structural parameter values for the best-fit monotartrate model and the three best-fit bitartrate models. *d* values are bondlengths, *x*, *y* and *z* are coordinates of O emitter atoms relative to the nearest-neighbour Cu atom, and of these surface Cu atoms relative to their positions in an ideal bulk-termination, along, respectively, $[1\bar{1}0]$, [001] and the outward surface normal, [110]. $\theta_{(COO)}$ and $\varphi_{(COO)}$ are the tilt and twist angles of the COO plane relative to, respectively, the surface normal and the $[1\bar{1}0]$ direction. $\varphi_{tartaric}$ is the rotation angle of the complete molecule about its centre relative to the surface normal; when $\varphi_{tartaric} = \varphi_{(COO)} = 0°$, the vector between the O atoms of the carboxylic acid group is along $[1\bar{1}0]$.

	monotartrate	bitartrate 'upright' hollow	bitartrate 'flat' hollow	bitartrate bridge
R-factor	0.32	0.45	0.43	0.43
$d_{Cu\text{-}O(1)}$ (Å)	1.92±0.08	1.94±0.06	1.93±0.08	1.94±0.07
$d_{Cu\text{-}O(2)}$ (Å)	1.93±0.06	1.95±0.09	1.95±0.08	1.97±0.09
$z_{O(1)}$ (Å)	1.84±0.06	1.89±0.08	1.78±0.08	1.86±0.08
$z_{O(2)}$ (Å)	1.89±0.06	1.86±0.08	1.85±0.08	1.77±0.08
$x_{O(1)}$ (Å)	0.1(+0.3/-0.1)	0.2±0.2	0.6±0.1	-0.4±0.1
$y_{O(1)}$ (Å)	-0.6(+0.6/-0.4)	0.4±0.2	-0.4±0.2	-0.4(+0.2/-0.3)
$x_{O(2)}$ (Å)	-0.4±0.4	-0.3±0.1Å	0.3±0.1	-0.8±0.1
$y_{O(2)}$ (Å)	0.2(+0.2/-0.3)	-0.5±0.2Å	-0.5±0.3	-0.4(+0.6/-0.2)
$\theta_{(COO)}$ (°)	17±6	38±6	70±10	70±10
$\varphi_{(COO)}$ (°)	20±10	2±4	-1±3	-2(+4/-2)
$\varphi_{tartaric}$ (°)	--	23±4	5±5	0±3
$d_{O\text{-}O}$ (Å)	2.2±0.1	2.2±0.1	2.2±0.1	2.2±0.1
$z_{Cu\{O(1)\}}$ (Å)	0.0±0.1	-0.1±0.1	-0.1±0.2	-0.1±0.1
$z_{Cu\{O(2)\}}$ (Å)	0.0±0.1	0.1±0.1	0.0±0.1	0.0±0.1
$y_{Cu\{O(1)\}}$ (Å)	--	0.0±0.4	0.1±0.3	0.1±0.4
$y_{Cu\{O(2)\}}$ (Å)	--	0.0±0.3	0.0±0.3	0±1

References

1 W.S. Knowles, Angew. Chem. Int. Ed., 41 (2002) 1998.

2 W.F. Kean, C.J.L. Lock, H.E. Howard-Lock, Lancet, 338 (1991) 1565.

3 J.A. Groenewegen, W.M.H. Sachtler, J. Catal., 38 (1975) 501.

4 A. Hoek, W.M.H. Sachtler, J. Catal., 58 (1979) 276.

5 Y. Izumi, Adv. Catal., 32 (1983) 215.

6 L. Pasteur, Annal Chim Phys, 24 (1848) 442.

7 M.Ortega Lorenzo, S. Haq, T. Bertrams, P. Murray, R. Raval, C.J. Baddeley, J. Phys. Chem. B, 103 (1999) 10661.

8 M.Ortega Lorenzo, C.J. Baddeley, C. Muryn, R. Raval, Nature 404 (2000) 376.

9 L.A.M.M. Barbosa, P. Sautet, J. Am. Chem. Soc., 123 (2001) 6639.

10 C.G.M. Hermse, A.P. van Bavel, A.P.J. Jansen, L.A.M.M. Barbosa, P. Sautet, R.A. van Santen, J Phys Chem B, 108 (2004) 11035.

11 J. Zhang, T. Lu, C. Jiang, J. Zou, F. Cao, Y. Chen, J Chem Phys, 131 (2009) 144703.

12 M.D. Crapper, C.E. Riley, D.P. Woodruff, Surf. Sci. 184 (1987) 121.

13 D.P. Woodruff, C.F.McConville, A.L.D.Kilcoyne, Th.Lindner, J.Somers, M.Surman, G.Paolucci, A.M.Bradshaw, Surf. Sci. 201 (1998) 228.

14 D. Kreikemeyer Lorenzo, W. Unterberger, D.A. Duncan, M.K. Bradley, T.J. Lerotholi, J. Robinson, D.P. Woodruff, Phys. Rev. Lett., 107 (2011) 046102.

15 K.-U. Weiss, R.Dippel, K-M.Schindler, P.Gardner, V.Fritzsche, A.M.Bradshaw, A.L.D.Kilcoyne, D.P.Woodruff , Phys. Rev. Lett. 69 (1992) 3196.

16 M. Pascal, C.L.A. Lamont, M. Kittel, J.T. Hoeft, R. Terborg, M. Polcik, J.H. Kang, R.Toomes, D.P. Woodruff, Surf. Sci. 492 (2001) 285.

17 J.-H. Kang, R. L. Toomes, M. Polcik, M. Kittel, J.-T Hoeft, V. Efstathiou, D. P. Woodruff, A. M. Bradshaw, J.Chem.Phys. 118 (2003) 6059.

18 D.I. Sayago, M. Polcik, G. Nisbet, C.L.A. Lamont, D.P. Woodruff, Surf. Sci. 590 (2005) 76.

19 D. P. Woodruff, A M Bradshaw, Rep. Prog. Phys., 57 (1994) 1029.

20 D. P. Woodruff, Surf Sci Rep, 62 (2007) 1

21 M.R. Weiss, R. Follath, K.J.S. Sawhney, F. Senf, J. Bahrdt, W. Frentrup, A. Gaupp, S. Sasaki, M. Scheer, H.C. Mertins, D. Abramsohn, F. Schäfers, W. Kuch, W. Mahler, Nucl. Instrum. Meth. A, 467-468 (2001) 449.

22 D.A. Duncan, M.K. Bradley, T.J. Lerotholi, D. Kreikemeyer Lorenzo, W. Unterberger, D.P. Woodruff, to be published

23 F. Gao, Z. Li, Y. Wang, L. Burkholder, W.T. Tysoe, J. Phys. Chem. C., 111 (2007) 9981.

24] T. Eralp, A. Shavorskiy, Z. Zheleva, G. Held, N. Kalashnyk, Y. Ning, T. Lineroth, Langmuir, 26 (2010) 18841.

25 M. Polcik, F. Allegretti, D.I. Sayago, G. Nisbet , C.L.A. Lamont, D.P. Woodruff, Phys. Rev. Lett. 92 (2004) 236103.

26 G. Jones, L.B. Jones, F. Thibault-Starzyk, S.E. A, R. Raval, S.J. Jenkins, G. Held, Surf. Sci., 600 (2006) 1924,

27 V. Fritzsche, J. Phys.: Condens. Matter, (1990) 1413.

28 V. Fritzsche, Surf. Sci., 265 (1992) 187

29 V. Fritzsche, Surf. Sci., 213 (1989) 648

30 J.B. Pendry, J. Phys. C, 13 (1980) 937

31 D.A. Duncan, J.I.J. Choi, D.P. Woodruff, Surf. Sci. 606 (2012) 278.

32 N.A. Booth, R. Davis, R. Toomes, D.P. Woodruff, C. Hirschmugl, K.M. Schindler, O. Schaff, V. Fernandez, A. Theobald, P. Hofmann, R. Lindsay, T. Gießel, P. Baumgärtel, A.M. Bradshaw, Surf. Sci., 387 (1997) 152.

33 F. Stern, C.A. Beevers, Acta Cryst., 3 (1950) 341.